Advanced Fiber Materials (2024) 6:1616–1628
https://doi.org/10.1007/s42765-024-00441-5

RESEARCH ARTICLE

Optimization of Wet-Spun PEDOT:PSS Fibers for Thermoelectric Applications Through Innovative Triple Post-treatments

Yu-Yu Deng[1] · Xiao-Lei Shi[2] · Ting Wu[1] · Yicheng Yue[2,3] · Wei-Di Liu[2] · Meng Li[2] · Fang Yue[3] · Pei Huang[1] · Qingfeng Liu[1] · Zhi-Gang Chen[2]

Received: 17 April 2024 / Accepted: 23 May 2024 / Published online: 21 June 2024

Abstract
Owing to the high flexibility, low thermal conductivity, and tunable electrical transport property, poly(3,4-ethylenedioxythiophene):poly(styrenesulfonate) (PEDOT:PSS) exhibits promising potential for designing flexible thermoelectric devices in the form of films or fibers. However, the low Seebeck coefficient and power factor of PEDOT:PSS have restricted its practical applications. Here, we sequentially employ triple post-treatments with concentrated sulfuric acid (H_2SO_4), sodium borohydride ($NaBH_4$), and 1-ethyl-3-methylimidazolium dichloroacetate (EMIM:DCA) to enhance the thermoelectric performance of flexible PEDOT:PSS fibers with a high power factor of (55.4 ± 1.8) μW m^{-1} K^{-2} at 25 °C. Comprehensive characterizations confirm that excess insulating PSS can be selectively removed after H_2SO_4 and EMIM:DCA treatments, which induces conformational changes to increase charge carrier mobility, leading to enhanced electrical conductivity. Simultaneously, $NaBH_4$ treatment is employed to adjust the oxidation level, further optimizing the Seebeck coefficient. Additionally, the assembled flexible fiber thermoelectric devices show an output power density of (60.18 ± 2.79) nW cm^{-2} at a temperature difference of 10 K, proving the superior performance and usability of the optimized fibers. This work provides insights into developing high-performance organic thermoelectric materials by modulating polymer chains.

Keywords Thermoelectric · PEDOT:PSS · Fiber · Wet spin · Post-treatment

1 Introduction

The flourishing development of intelligent wearable electronic products has significantly increased the demand for flexible wearable devices in many fields such as soft robotics, medical diagnostic equipment, and smartwatches [1]. Wearable flexible thermoelectric devices (TEDs), having the capability to directly convert thermal energy into electrical energy, can harness the temperature difference between the human body and the environment to achieve sustainable power generation, providing an effective solution for the development of wearable energy supply systems [2]. As a core component of wearable flexible TEDs, it is crucial to secure high thermoelectric performance in flexible thermoelectric materials. Generally, higher thermoelectric performance in these materials leads to higher energy conversion efficiency of the device. Therefore, the focus on developing thermoelectric materials with high performance, flexibility, and stability is of paramount importance. Their thermoelectric performance is evaluated using the dimensionless figure-of-merit ZT, which is defined as $ZT = S^2\sigma T/\kappa$, where S denotes the Seebeck coefficient, σ represents the electrical conductivity, T is the absolute temperature, and κ represents the thermal conductivity [3–5]. The power factor ($S^2\sigma$) is also employed to assess the thermoelectric potential of materials, particularly when the κ of flexible thermoelectric materials is challenging to accurately measure.

Yu-Yu Deng and Xiao-Lei Shi contributed equally to this work.

✉ Qingfeng Liu
qfliu@njtech.edu.cn

✉ Zhi-Gang Chen
zhigang.chen@qut.edu.au

[1] State Key Laboratory of Materials Oriented Chemistry Engineering, College of Chemistry Engineering, Nanjing Tech University, Nanjing 211816, Jiangsu, People's Republic of China

[2] School of Chemistry and Physics, ARC Research Hub in Zero-Emission Power Generation for Carbon Neutrality, and Centre for Materials Science, Queensland University of Technology, Brisbane, QLD 4000, Australia

[3] Merino & Co Ltd, Osborne Park, Perth, WA 6017, Australia

To meet the high flexibility requirements of wearable TEDs, thermoelectric materials need significant flexibility. Thin film and fiber-based thermoelectric materials have gained increasing attention from researchers due to their excellent flexibility, lightweight, and comfortable wearability [6, 7]. Particularly, in comparison to thin film materials, fiber materials offer better weaveability and broader application potential [6]. In recent years, various types of thermoelectric fiber materials have been developed, including organic fibers, inorganic fibers, and organic/inorganic hybrid fibers. Compared to inorganic fibers, organic polymerized fibers hold advantages such as low κ, nontoxicity, low cost, and good environmental stability [8]. Specifically, poly(3,4-ethylenedioxythiophene):poly(styrenesulfonate) (PEDOT:PSS) has been extensively studied due to its highly tunable σ, good solution processability, and excellent biocompatibility [9]. However, the original PEDOT:PSS displays a relatively low σ of around 2 S cm^{-1} and S of $\leq$ 14 μV K^{-1}, leading to insufficient $S^2\sigma$ to meet the growing demands of device performance [10, 11]. Therefore, to address these problems, the main research focus is to explore appropriate pre-treatments or post-treatments, along with reasoned doping or dedoping strategies, to enhance the $S^2\sigma$ of PEDOT:PSS [12–15]. Additionally, composite carbon materials such as carbon nanotubes (CNTs) and inorganic materials like nanoscale semiconductors can effectively filter out low-energy charge carriers through energy filtering, thereby enhancing the S [16, 17]. For instance, PEDOT:PSS fibers have been prepared via wet spinning, followed by post-treatment with sulfuric acid (H_2SO_4). Owing to the effective post-treatment and confinement effect, the prepared fibers have a high σ of 4029.5 S cm^{-1} [18]. However, these techniques are still limited to achieving high thermoelectric capabilities of PEDOT:PSS fibers. Therefore, it is still needed to explore effective and stable methods to obtain high-performance PEDOT:PSS thermoelectric fibers.

Ionic liquids (ILs) have attracted widespread attention due to their high ionic conductivity, thermal stability, antibacterial properties, and excellent solubility [19–23]. In recent years, using ionic liquids as agents to enhance the thermoelectric performance of organic materials has become a popular research topic. For example, it has been reported that PEDOT:PSS fibers can be fabricated by combining with 1-ethyl-3-methylimidazolium dicyanamide (EMIM:DCA) [24]. The observed high thermoelectric performance in PEDOT:PSS/EMIM:DCA fibers is mainly attributed to the synergistic effects of sulfuric acid, ionic liquid, and high tensile strength, which induces the substantial elimination of PSS and the high crystallinity and orientation of PEDOT [24–26]. However, to date, there is still a lack of high-performance thermoelectric fibers and reliable mechanistic analysis. Moreover, the composite applications of ionic liquid treatment and conventional pre- and post-treatment are currently unexplored.

In this study, a triple post-treatment method, including H_2SO_4, sodium borohydride ($NaBH_4$), and 1-ethyl-3-methylimidazolium dichloroacetate (EMIM:DCA), was developed to be applied to the PEDOT:PSS fibers, prepared via wet spinning method. After this triple post-treatment, the thermoelectric performance of the fibers was significantly enhanced. From a series of structural characterizations and thermoelectric performance evaluation, the underlying mechanism for its performance improvement has been illustrated. Additionally, the assembled flexible TEDs using the as-prepared thermoelectric fibers show excellent capability for generating electricity from temperature differences. This work provides new insights into the performance optimization mechanism and expanded applications of organic thermoelectric fibers.

2 Experimental Section

2.1 Materials and Chemicals

PEDOT:PSS solution (Clevios PH1000) was purchased from Heraeus. Dimethyl sulfoxide (DMSO) (AR) was purchased from Shanghai Macklin Biochemical CO., LTD. Isopropanol (IPA) (AR, 99.8%) was purchased from Energy Chemical Reagent CO., LTD. Ethanol absolute was purchased from Shanghai Lingfeng Chemical Reagent CO., LTD. H_2SO_4 (AR, 98.08%) was purchased from Shanghai Lingfeng Chemical Reagent CO., LTD. $NaBH_4$ (AR, ≥ 97%) was purchased from Shanghai Lingfeng Chemical Reagent CO., LTD. EMIM:DCA (98%) was purchased from Shanghai Macklin Biochemical CO., LTD. Methanol (CH_3OH) (≥ 99.7%) was purchased from Sinopharm Chemical Reagents CO., LTD.

2.2 Wet spinning of PEDOT:PSS fibers

First, the PEDOT:PSS dispersion with 5 wt% DMSO was concentrated to 2.5 wt% under magnetic stirring at 90 °C for 1 h. Then, the PEDOT:PSS fibers were prepared at room temperature using a wet spinning setup. Typically, 200 μL of the spinning formulation was loaded into a 5 mL syringe. The formulation was extruded through a microneedle into an IPA coagulation bath, which was fixed on a rotation stage. The diameters of the microneedles were 27 G. The flow rate of the spinning formulation was maintained at 15 μL min^{-1} by a syringe pump (LSP01-2A). The rotation stage was to pre-stretch the as-spun fibers and simultaneously avoid the adhesion between fibers in a wet state. After extrusion, the as-spun fibers were collected at the bottom of the coagulation bath and then rinsed in a washing bath consisting of

ethanol/ deionized (DI) water (v/v, 1/1) two times. Finally, the fibers were dried by hanging them in the air above a heating table. The samples were named P/D (PEDOT:PSS/DMSO).

2.3 Triple Post-Treatment

Firstly, the P/D samples were immersed in H_2SO_4 for 1–4 h at room temperature. Then, the H_2SO_4-treated samples were further treated with a $NaBH_4$ solution. Considering the strong reducibility of $NaBH_4$, a 1 mol/L $NaBH_4$ solution was prepared before the treatment. Then the H_2SO_4-treated samples were immersed in concentrated H_2SO_4 at room temperature. Finally, the H_2SO_4-$NaBH_4$-treated samples were immersed in EMIM:DCA/CH_3OH solution at room temperature for 1–6 h. All the post-treatment samples were rinsed in deionized water two times to wash away the remnant solvent and dried on a heating table at 65 °C for 10 min. For simplicity, the sample treated only by H_2SO_4 was labeled as H_2SO_4-treated sample, the sample treated by H_2SO_4 and $NaBH_4$ was labeled as H_2SO_4-$NaBH_4$-treated sample, and the sample treated by H_2SO_4, $NaBH_4$, and EMIM:DCA/CH_3OH was labeled as H_2SO_4-$NaBH_4$-EMIM:DCA/CH_3OH-treated sample.

2.4 Thermoelectric Device Fabrication

The fibrous TEDs were assembled using the H_2SO_4-$NaBH_4$-EMIM:DCA/CH_3OH PEDOT:PSS fibers and nickel (Ni) wires (diameter: 0.05 mm) as the p- and n-legs, respectively. One pair of the p-n thermoelectric legs was connected on polyimide (PI) which was stuck on a flexible poly(ethylene terephthalate) (PET) substrate. The joints between H_2SO_4-$NaBH_4$-EMIM:DCA/CH_3OH PEDOT:PSS fibers and Ni wires were connected using silver paste. The Cu wires were connected at the end of the thermoelectric generator to measure output properties.

2.5 Measurement and Characterization

The σ of the fibers was measured by the four-point-probe method using a source meter (Keithley 2450). The samples were prepared by placing the fiber on a glass slide and four areas of fiber are coated with silver paste for probe contact. The corresponding electrical conductivities were calculated using Eq. (1):

$$\sigma = \frac{L}{RA}, \tag{1}$$

where R (Ω) is the electrical resistance, A (cm^2) is the cross-sectional area, and L (cm) is the distance between electrodes. The S data of the samples were measured at room temperature with the portable Seebeck coefficient tester (PTM-3). The tensile properties of fibers were measured by a YG001E tensile tester (the pre-tightening force is 0.01 N, the gauge length is 20 mm, and the extension rate is 2 mm/min). For the above thermoelectric and mechanical measurements, at least 10 samples from the same batch of fibers were tested. The values presented in this work are the average values which are rounded to two decimal places, and the error bars are the standard deviation between samples from the same batch of fibers.

The crystallinity of samples was investigated by X-ray diffraction (XRD, Smartlab) using Cu K_α radiation at room temperature. The surface morphology and cross-sectional morphologies of the fibers were conducted on field emission scanning electron microscopy (FESEM, JEOL-S4800), and tabletop optical microscopy (Hitachi TM3000). The oxidation levels of the samples were characterized by ultraviolet and visible absorption spectrum (UV–Vis absorption spectrum, Lambda 950) and X-ray photoelectron spectroscopy (XPS, Thermo ESCALAB 250, Japan) using monochromatic Al K_α radiation. Raman spectroscopy was performed from 1200 to 1800 cm^{-1} on a confocal Raman microscope (LabRAM HR Evolution) using a 553 nm laser. The open-circuit voltage (V_{OC}) of the device was measured using a data acquisition/multimeter system (Keithley DAQ6510) and a Keithley 2450. A resistor box (0–9000 Ω) was used to act as an external resistor and a thermocouple was used to measure the temperature difference when testing the output power of the device.

3 Results and Discussion

We initially concentrated the PEDOT:PSS spinning solution by adding 5% DMSO and prepared PEDOT:PSS fibers utilizing the wet spinning method. Subsequently, we applied a triple post-treatment with H_2SO_4, $NaBH_4$, and EMIM:DCA to adjust the thermoelectric performance of the PEDOT:PSS fibers, as illustrated in Fig. 1a. The prepared fibers ultimately exhibited an optimum $S^2\sigma$ value of (55.4 ± 1.8) μW m^{-1} K^{-2}, demonstrating strong competitiveness compared to the reported literature [18, 25, 27–31], as depicted in Fig. 1b. After triple post-treatment, an optimal balance between σ and S factors for peak power can be achieved. Based on this, fibers treated with the H_2SO_4-$NaBH_4$-EMIM:DCA triple combination were utilized to manufacture a flexible TED on PI. The TED exhibited a power density of (60.18 ± 2.79) nW cm^{-2} at a temperature difference ΔT of 10 K, demonstrating the potential of designed PEDOT:PSS fibers for application in wearable TEDs.

To obtain high-quality pristine PEDOT:PSS fibers, 5 wt% polar solvent DMSO was introduced into the spinning solution. We first investigated the influence of H_2SO_4 on the σ and S of PEDOT:PSS fibers by the wet spinning method.

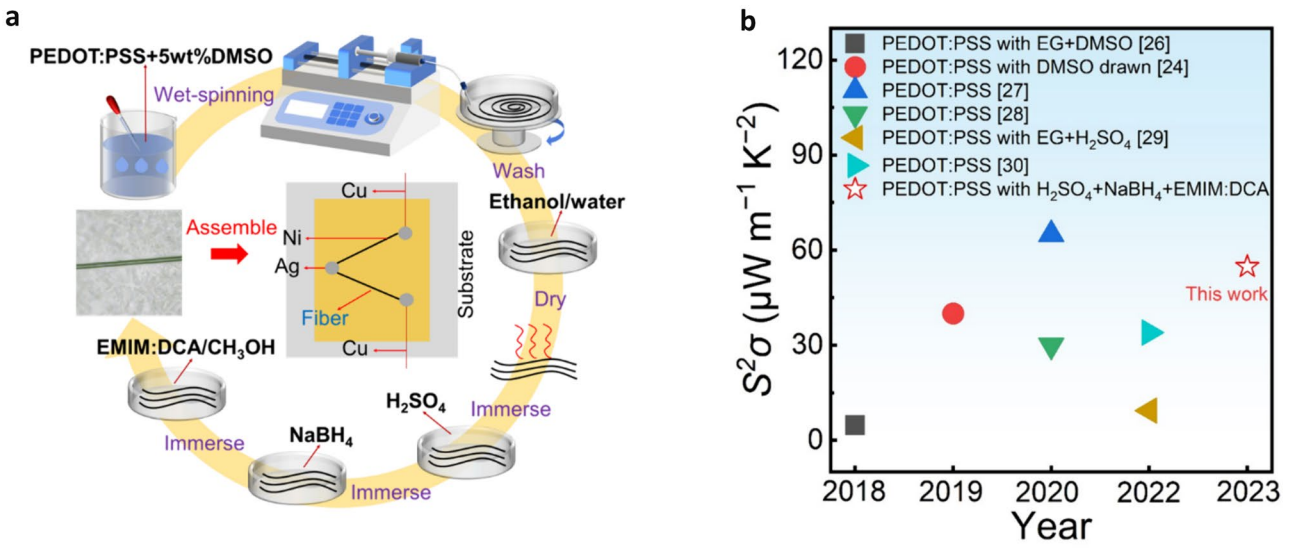

Fig. 1 Introduction of optimizing wet-spun PEDOT:PSS fibers for thermoelectric applications through innovative triple post-treatments. **a** Schematic diagram of preparing poly(3,4-ethylenedioxythiophene): poly(styrenesulfonate) (PEDOT:PSS) fibers post-treated with sulfuric acid (H_2SO_4), sodium borohydride ($NaBH_4$), and 1-ethyl-3-methylimidazolium dichloroacetate/Methanol (EMIM:DCA/CH_3OH) solution and the thermoelectric device (TED). The photograph of the as-achieved free-standing PEDOT:PSS fiber was treated with H_2SO_4 and 1 mol L^{-1} $NaBH_4$ and 20% EMIM:DCA/CH_3OH solution. **b** Comparison of power factor $S^2\sigma$ between this work and reported post-treated PEDOT:PSS fibers [18, 25, 27–31]

Figure 2a displays the variations in the measured σ, S, and the calculated $S^2\sigma$ of PEDOT:PSS fibers with changing H_2SO_4 post-treatment duration. The untreated PEDOT:PSS fibers only exhibit a low σ of (195.3 ± 43.5) S cm^{-1} and an S of (15.4 ± 0.4) μV K^{-1}. As the post-treatment time extended to 2 h, the σ is significantly increased to (1813.7 ± 182.3) S cm^{-1}, while the S remains essentially constant. Figure 2b illustrates the relationship between the measured σ, S, and calculated $S^2\sigma$ of PEDOT:PSS fibers and the post-treatment duration with $NaBH_4$. With the increasing $NaBH_4$ treatment duration, most samples exhibit a notable increase in S and a decrease in σ. The fibers treated with 1 mol L^{-1} $NaBH_4$ show the maximum S, reaching (20.8 ± 0.8) μV K^{-1}. Figure 2c depicts the σ, S, and determined $S^2\sigma$ of PEDOT:PSS fibers measured under varying EMIM:DCA post-treatment durations after 2 h of H_2SO_4 treatment and 0.5 h of $NaBH_4$ treatment. With the increasing treatment duration, the σ is gradually increased, while the S shows a slight decrease. For PEDOT:PSS fibers treated with H_2SO_4-$NaBH_4$-EMIM:DCA/CH_3OH for 4 h, the optimal σ is (1395.5 ± 31.5) S cm^{-1}. Compared to the reported results summarized in Table S1, the maximum $S^2\sigma$ is (55.4 ± 1.8) μW m^{-1} K^{-2} with the optimal post-treatment time. A shorter treatment duration may not be sufficient for EMIM:DCA to interact adequately with the PEDOT:PSS chain, while prolonging the treatment time may lead to excessive oxidation of PEDOT [16, 18, 26]. Figure S1 in the Supporting Information illustrates the relationship between the measured σ, S, and determined $S^2\sigma$ of

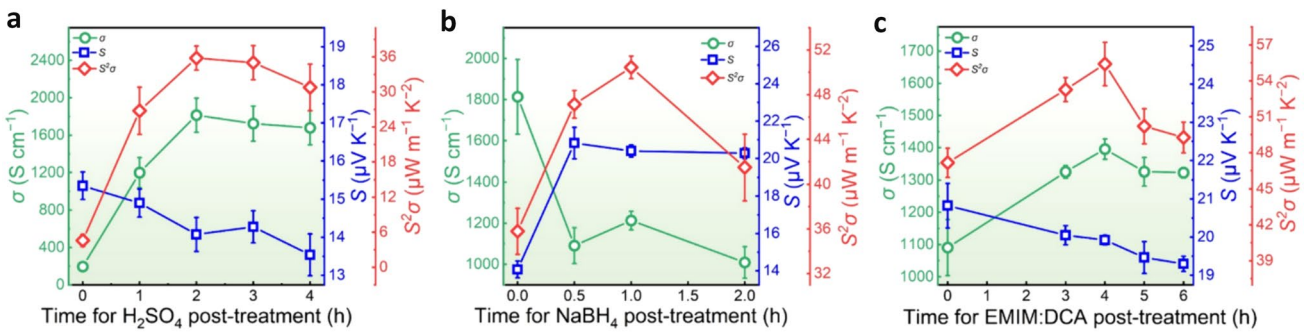

Fig. 2 Thermoelectric properties of fibers. Measured room-temperature electrical conductivity σ, Seebeck coefficient S, and $S^2\sigma$ of PEDOT:PSS fibers treating with **a** H_2SO_4, **b** 1 mol L^{-1} $NaBH_4$, and **c** 20% EMIM:DCA/CH_3OH solution as a function of treating duration

PEDOT:PSS fibers and the $NaBH_4$ post-treatment time after 2 h of H_2SO_4 treatment and 1 h of $NaBH_4$ treatment. With the increasing EMIM:DCA treatment time, most samples show a rise in σ and a decline in S, with the maximum $S^2\sigma$ of (45.7 ± 2.8) μW m^{-1} K^{-2}. Based on these conclusions, the triple post-treatment with H_2SO_4, $NaBH_4$, and EMIM:DCA/CH_3OH solution can effectively enhance the σ and S of PEDOT:PSS fibers.

To understand the mechanism of the triple post-treatment with H_2SO_4, $NaBH_4$, and EMIM:DCA/CH_3OH solutions that improve the thermoelectric properties of PEDOT:PSS fibers, we conducted morphological characterization using SEM. Figure S2a–d in the Supporting Information displays the SEM images of pristine PEDOT:PSS fibers without and with H_2SO_4 treatment, H_2SO_4-$NaBH_4$ treatment, and H_2SO_4-$NaBH_4$-EMIM:DCA/CH_3OH treatments. The fibers treated with H_2SO_4 underwent a 2-h post-treatment. The fibers subjected to dual treatment were treated with $NaBH_4$ for 30 min, followed by a 2-h treatment with H_2SO_4. The fibers undergoing triple treatment were treated with EMIM:DCA/CH_3OH solution and then with 2 h of H_2SO_4 treatment and 0.5 h of $NaBH_4$ treatment. The prepared fibers exhibit a cylindrical shape and uniform thickness without significant irregularities.

Figure 3a–d displays the typical SEM images of pristine fibers (abbreviated as P/D) and the fibers subjected to H_2SO_4 treatment at different magnifications. After the H_2SO_4 treatment, the fiber diameter was significantly decreased from 17.9 to 9.5 μm, and meanwhile, the fiber surface became rougher with increased wrinkles. It is evident that the wrinkles of PEDOT:PSS are well aligned in the direction of the fiber, indicating the submicron-scale orientation of PEDOT:PSS clusters [18]. It has been reported that H_2SO_4 is one of the most effective agents for improving thermoelectric performance, especially in electrical conductivity of PEDOT-based derivatives [18, 26, 27, 32]. Figure 3e–f shows SEM images of fibers treated with H_2SO_4-$NaBH_4$ at different magnifications. The diameter and roughness of the fibers barely changed after H_2SO_4-$NaBH_4$ treatment. This suggests that $NaBH_4$ treatment has no significant influence on the elimination of the PSS chains. More morphological details can be referred to Figure S3 in the Supporting Information.

Figure 4a–c displays SEM images of cross-sectional views of fibers treated with H_2SO_4-$NaBH_4$-EMIM:DCA/CH_3OH at different magnifications. As can be seen, the fiber diameter was slightly decreased to 9.1 μm. The internal structure of the fibers along the cross-sectional direction also showed a well-organized arrangement, indicating that the ionic liquid EMIM:DCA treatment further removed the insulating PSS chains. More morphological details are described in Figures S4–5 in the Supporting Information. To further understand the mechanism by which the triple post-treatment improves the thermoelectric properties of PEDOT:PSS fibers, we conducted XRD, Raman spectroscopy, UV–Vis absorption spectroscopy, and XPS to investigate the structural changes. Figure 4d–e illustrates the XRD and Raman spectra of pristine fiber, and the fibers treated with H_2SO_4, H_2SO_4-$NaBH_4$, and H_2SO_4-$NaBH_4$-EMIM:DCA/CH_3OH. For the XRD results, a characteristic peak was observed around 6.6° in the pristine fibers, corresponding to the alternate arrangement of layers on the (100) planes of PEDOT and PSS [25, 33–35]. Through H_2SO_4 treatment, H_2SO_4-$NaBH_4$ treatment, and H_2SO_4-$NaBH_4$-EMIM:DCA/CH_3OH treatment, the peak at around 6.6° became sharper, indicating an increase in fiber crystallinity due to the efficient elimination of PSS [36, 37]. This is consistent with the SEM results. Crystallinity determines the effectiveness of charge transfer within the conjugated polymer crystalline domains and thus exhibits high electrical performance [8]. Such behavior of charge carriers within the domains is similar to that of metals, resulting in more effective charge carrier transport.

Figure 4e displays the Raman spectra of the fibers untreated and treated with H_2SO_4, H_2SO_4-$NaBH_4$, and H_2SO_4-$NaBH_4$-EMIM:DCA/CH_3OH, respectively. The Raman peaks between 1400 $cm^{-1}$and 1500 cm^{-1} are attributed to the stretching vibrations of $C_\alpha = C_\beta$ on the thiophene rings of the PEDOT chain [38–40]. For pristine fibers, the characteristic absorption peak of PEDOT is observed at 1428 cm^{-1}. The redshift of approximately 8 cm^{-1} observed in the peak at 1428 cm^{-1} after H_2SO_4 treatment demonstrates a transformation of the molecular conformation of PEDOT from a helical benzoid to a linear quinoid conformation [8]. Following dual treatment with H_2SO_4 and $NaBH_4$, the Raman peak shifts from 1420 cm to 1424 cm^{-1}. This is correlated with the deformation of the main chain during the chemical reduction process of polarons and neutral states and the transition between benzoid and quinoid types [37, 41]. After the treatment with EMIM:DCA/CH_3OH solution, the Raman peak at 1424 cm^{-1} undergoes a redshift of around 6 cm^{-1}. This indicates that the oxidation of the PEDOT molecules [8] has been reduced to a benzoid structure by $NaBH_4$, back to a tilted quinoid structure, as shown in Fig. 4f. Benzoid and quinoid structures, which are two resonance forms, emerge from sp2-hybridized carbon atoms and conjugated chain segments in thiophene-based conjugated polymers. The curled conformation is favored by the benzoid structure, leading to a deviation of adjacent thiophene rings from each other because of the presence of relatively flexible C–C bonds. In contrast, the quinoid structure is constrained by stiff conjugated C = C bonds, forming a relatively broad and flat structure in the PEDOT main chain, and hence, it is the preferred structure for extending the curled configuration [38, 39, 42, 43]. Additionally, charge carriers often concentrate in the benzoid structure,

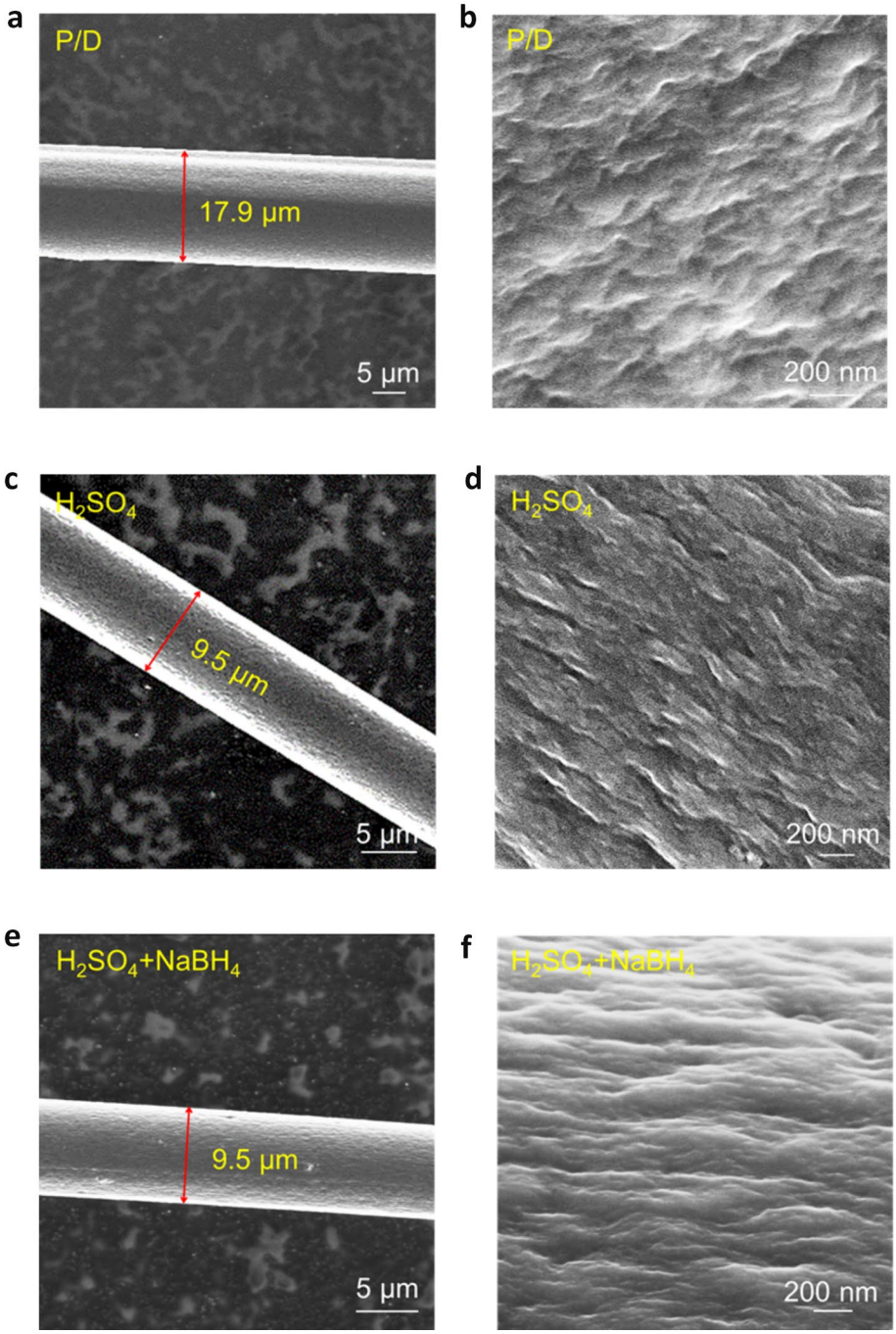

Fig. 3 Scanning electron microscopy (SEM) images of fibers. SEM images of a PEDOT:PSS fiber pre-treated with dimethyl sulfoxide (DMSO) (abbreviated as P/D) in **a** low and **b** high magnifications. SEM images of an H_2SO_4-treated PEDOT:PSS fiber with a treatment duration of 2 h in **c** low and **d** high magnifications. SEM images of a $NaBH_4$-treated PEDOT:PSS fiber with a treatment duration of 0.5 h in **e** low and **f** high magnifications

whereas the uncurled structure in the quinoid type, resulting from the weaker binding between thiophene rings along the conjugated chain, facilitates charge carriers to move along their directional movement.

Figure 4g presents the XPS results of the S2p for PEDOT:PSS fibers. The peaks detected at 166–172 and 161–166 eV in the S2p XPS spectra can be attributed to sulfur atoms in PSS and PEDOT, respectively [27, 44–46]. Therefore, the ratio of PSS to PEDOT can be determined

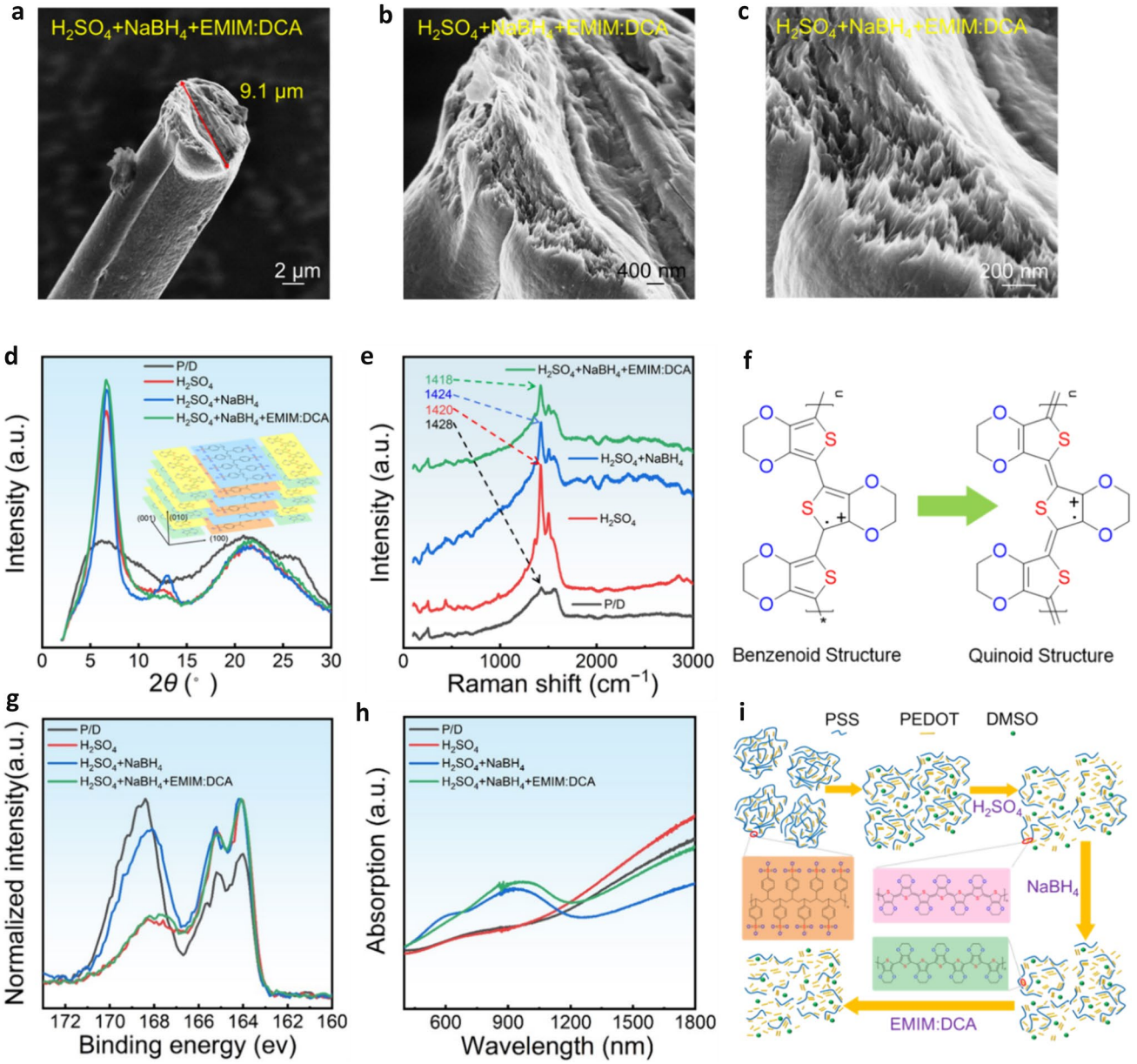

Fig. 4 SEM images, X-ray diffraction (XRD) patterns, Raman spectra, X-ray photoelectron spectroscopy (XPS) patterns, and ultraviolet and visible (UV–Vis) absorption spectra of fibers. Cross-sectional SEM images of an EMIM:DCA/CH_3OH-treated PEDOT:PSS fiber with a treatment duration of 4 h in **a** low, **b** medium, and **c** high magnifications. **d** XRD patterns and **e** Raman spectra of P/D, H_2SO_4-treated, H_2SO_4-$NaBH_4$-treated, and H_2SO_4-$NaBH_4$-EMIM:DCA/CH_3OH-treated PEDOT:PSS fibers. The inset in **d** illustrates the structure of PEDOT:PSS. **f** Schematic models of the transformation from the benzenoid structure to the quinoid structure. **g** XPS and **h** UV–Vis absorption spectra of P/D, H_2SO_4-treated, H_2SO_4-$NaBH_4$-treated, and H_2SO_4-$NaBH_4$-EMIM:DCA/CH_3OH-treated PEDOT:PSS fibers. **i** Illustration of the structural transition of PEDOT:PSS fibers during the triple post-treatments

based on the intensity ratio of the PSS peak to the PEDOT peak. During the first H_2SO_4 post-treatment, PEDOT:PSS undergoes an interaction with H_2SO_4 through the reaction $PSS^- + H_2SO_4 \rightarrow HSO_4^- + PSSH$, resulting in a significant decrease in the PSS/PEDOT ratio. The further reduction in the PSS/PEDOT ratio after treatment with EMIM:DCA/CH_3OH solution mainly results from the ion-exchange equilibrium reaction between EMIM:DCA and PEDOT:PSS, represented by PEDOT:PSS + EMIM:DCA $\rightarrow$ EMIM + PSS^- + PEDOT + DCA^-. After the triple treatment with H_2SO_4-$NaBH_4$-EMIM:DCA/CH_3OH, the PSS/PEDOT ratio was maximally decreased, demonstrating

effective removal of PSS, contributing to the formation of a more crystalline PEDOT structure within the fibers, thereby greatly enhancing the σ [18, 24, 32].

We also characterized the structural features and the chemical doping levels of all samples by UV–visible–NIR spectroscopy, as shown in Fig. 4h. Different oxidation states of PEDOT exhibit significant absorption at various wavelengths. Specifically, PEDOT chains display absorptions at around 600, 900, and 1400 nm in neutral, polaronic, and bipolaronic states, respectively [47, 48]. In undoped conjugated polymers, the neutral state is predominant, but it can transition to polaronic and bipolaronic states upon chemical or electrochemical oxidation [8, 49]. Regarding the band structure, polarons (bipolarons) generate localized electronic states within the bandgap by absorbing energy, leading to a localized upward shift of the highest occupied molecular orbital (HOMO) and a downward shift of the lowest unoccupied molecular orbital (LUMO) [50]. These newly formed localized electronic states are denoted as polaronic (bipolaronic) levels [50]. Compared to pristine fibers, the H_2SO_4-treated fibers show an increased spectral absorption at 1400 nm, indicating an elevated average oxidation level of the fibers. The H_2SO_4-$NaBH_4$-treated sample exhibits an increased absorption at 900 nm but a reduced absorption at 1400 nm, suggesting that a substantial amount of bipolarons have been reduced to polarons, and $NaBH_4$ can effectively reduce the oxidation state of PEDOT by facilitating the transition from the valence band to the conduction band [50]. This also explains why the σ was significantly decreased after $NaBH_4$ treatment following H_2SO_4 treatment. $NaBH_4$ can dedope PEDOT, localizing positive charges on PEDOT and reducing carrier concentration, leading to an increase in the *S*. Finally, the PEDOT:PSS fibers treated with H_2SO_4-$NaBH_4$-EMIM:DCA/CH_3OH show a significant increase in absorption related to polaronic and bipolaronic states, indicating an overall elevation in the oxidation level of the entire system, attributed to the transition from the occupied HOMO levels to the empty polaronic and bipolaronic levels [50]. In this case, the inter-chain coupling induces a transformation of the polaronic and bipolaronic states into corresponding band-like structures [50]. The connection of the two band-like structures reduces the band gap, making it easier for electronic charges to be delocalized and transported, similar to the behavior observed in metals [8].

Figure 4i illustrates the chemical structures of PEDOT and PSS, along with the inferred structures after triple treatments. Three corresponding mechanisms were employed to modify the chemical composition, polymer chain conformation, and oxidation level of PEDOT:PSS fibers, aiming to enhance both σ and *S*. The first mechanism involving polar solvents is well established. The original PEDOT:PSS is composed of a conductive core rich in PEDOT but insoluble, surrounded by an insulating hydrophilic PSS shell, where the PSS shell acts as a dopant to balance charges, improving the dispersing properties of PEDOT in water [31, 51, 52]. DMSO, a highly polar solvent, weakens the Coulombic attraction between PEDOT and PSS chains, which can effectively promote phase separation between PEDOT and the PSS shell [18, 25, 48, 53, 54]. The increase in σ is attributed, in part, to the second mechanism, selective removal of PSS relative to PEDOT. Internal treatment of PEDOT:PSS with H_2SO_4 and an ionic liquid, where the insulating PSS is selectively removed from PEDOT, results in the reorientation of PEDOT chains into a more conductive linear form [55–58]. H_2SO_4 and EMIM:DCA can undergo ion-exchange reactions with PEDOT:PSS, facilitating the well-organized arrangement of the conductive PEDOT chain within the fiber, reducing the potential barrier to transport charge carrier, and thereby enhancing the σ. The variation in *S* is mainly attributed to the third mechanism, which involves modulating the doping level of the PEDOT chains. The purpose of utilizing a strong reducing agent $NaBH_4$ solution in the post-treatment is to enhance the *S* of PEDOT:PSS by modifying the oxidation level. The reduction process is reversible, causing a reverse molecular structural transition from quinoid features to benzenoid features. After the synergistic action of H_2SO_4, $NaBH_4$, and EMIM:DCA/CH_3OH triple treatment, PEDOT exhibits a partial reduction leading to the enhancement in both σ and *S*, which aligns with the observed changes in thermoelectric performance as depicted in Fig. 2.

To fabricate fiber-based TEDs, it is imperative to utilize conductive fibers that possess high tensile strength and flexibility, ensuring their stability during the assembling or weaving process to prevent breakage [24]. Figure 5a illustrates the tensile strength and elongation characteristics of pristine, H_2SO_4-treated, H_2SO_4-$NaBH_4$-treated, and H_2SO_4-$NaBH_4$-EMIM:DCA/CH_3OH-treated PEDOT:PSS fibers. The results indicate a significant increase in tensile strength after H_2SO_4 treatment. Especially, the PEDOT:PSS fibers treated with H_2SO_4-$NaBH_4$-EMIM:DCA/CH_3OH exhibit approximately an increase of up to threefold higher tensile strength. Following multiple averaged tests, the calculated tensile strength and elongation of H_2SO_4-$NaBH_4$-EMIM:DCA/CH_3OH-treated PEDOT:PSS fibers were determined to be 458.2 MPa and 11%, respectively. Additionally, Fig. 5b presents the calculated Young's modulus of the fibers after various post-treatments, measuring the stiffness based on stress and elongation [24]. The Young's modulus of the prepared fibers exceeds 4.2 GPa for H_2SO_4-$NaBH_4$-EMIM:DCA/CH_3OH-treated PEDOT:PSS fibers. More detailed data are summarized in Table S2. These findings demonstrate that the fabricated fibers exhibit excellent flexibility, ensuring that fiber-based devices can offer superior comfort.

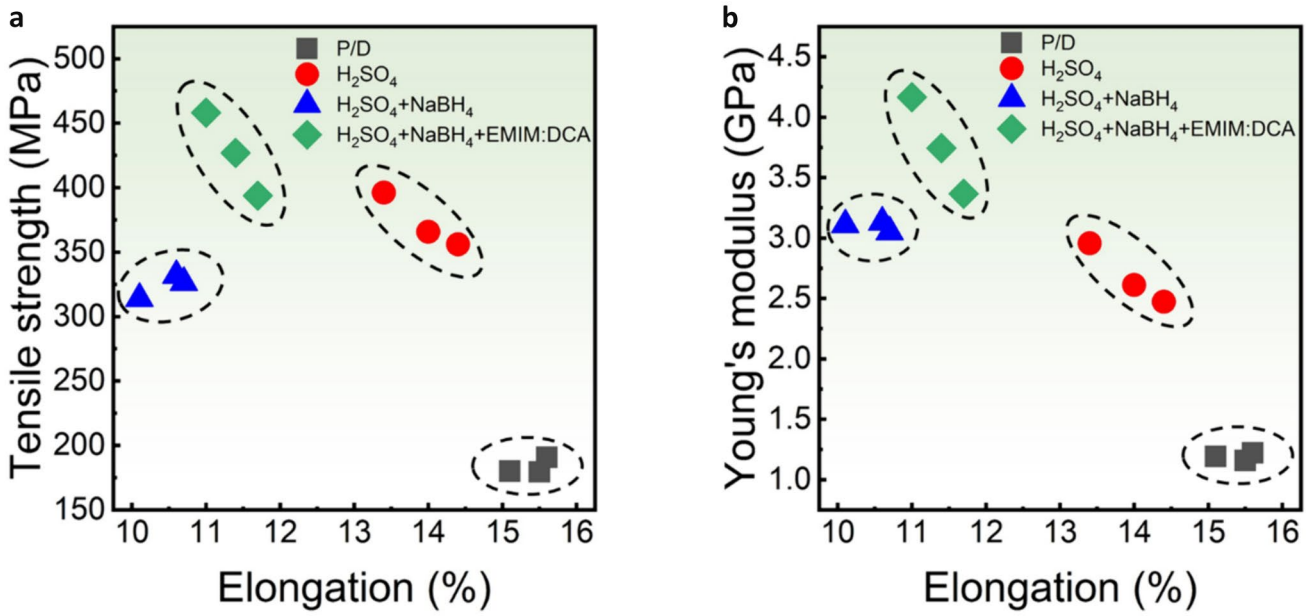

Fig. 5 Mechanical properties of fibers. **a** Tensile strength and **b** Young's modulus of P/D, H_2SO_4-treated, H_2SO_4-$NaBH_4$-treated, and H_2SO_4-$NaBH_4$-EMIM:DCA/CH_3OH-treated PEDOT:PSS fibers as a function of elongation

To assess the potential for practical use of the triple-treated fibers, a pair of fiber-based PEDOT:PSS-nickel (Ni) TED was designed, as illustrated in Fig. 6a–b. Utilizing the Seebeck effect, the fiber-based TED can convert thermal energy into electrical energy. Initially, a pair of 2-cm-long p-type PEDOT:PSS fibers and n-type Ni wires were attached to a flexible PI substrate. When the flexible TED was placed on a heating stage, one end exposed to the air acted as the cold side, while the other end close to the heating stage served as the hot side. The intersections of the fibers were connected with silver paste, and the external circuit was connected with high-conductivity copper wires, as shown in Fig. 6c–d. Due to the resistance of the fiber being close to 2000 Ω, the optimal connection involved parallelly connecting two voltmeters in the circuit to measure the output performance. The optimum output power was measured by adjusting the external resistance. Figure 6e illustrates the relationship between the V_{OC} and output power density of the TED at a ΔT of 10 K with varying load resistance. The effective device area is calculated using Eq. (2):

$$A_{\text{total}} = n \times \left(A_{\text{p-type}} + A_{\text{n-type}}\right), \tag{2}$$

where n is the number of thermocouples, and $A_{\text{p-type}}$ and $A_{\text{n-type}}$ represent the cross-sectional areas of the p-type and n-type legs, respectively [27, 59]. Based on the measured fiber diameter, the average effective device area per pair was calculated to be approximately 0.002 mm^2. It is noteworthy that the peak output power of the device is achieved when the internal load resistance matches the external load resistance [60–63]. The calculated maximum output power density at the ΔT of 10 K was (60.18 ± 2.79) nW cm^{-2}. Figure 6f plots the V_{OC} and output power density of the fiber-based TED as functions of ΔT using a heating stage. As ΔT increases from 5 to 25 K, V_{OC} increases from (0.12 ± 0.03) mV to (0.49 ± 0.02) mV, and the maximum power density increases from (0.027 ± 0.005) μW cm^{-2} to (0.28 ± 0.04) μW cm^{-2}. Figure 6g displays the measured output voltage of the PEDOT:PSS-Ni TED at a ΔT of 10 K. To exhibit the excellent flexibility and stability of the H_2SO_4-$NaBH_4$-EMIM:DCA/CH_3OH-treated fibers, the changes in the S and resistance R were recorded after repeated bending and straightening, as shown in Fig. 6h–i. The R was decreased by less than 5%, and the S remained unchanged after 1000 bending cycles, indicating high fatigue resilience [29]. The H_2SO_4-$NaBH_4$-EMIM:DCA/CH_3OH-treated PEDOT:PSS fibers prepared in our work can withstand repeated deformation without significant changes in electrical performance. Our findings suggest significant potential for sustainable charging in low-grade wearable electronic devices.

4 Conclusions

To manufacture flexible thermoelectric fibers with a high power factor, this study proposes a triple post-treatment of PEDOT:PSS fibers with H_2SO_4, $NaBH_4$, and EMIM:DCA/CH_3OH at room temperature. With optimized processing times, the σ is increased from (195.3 ± 43.5)

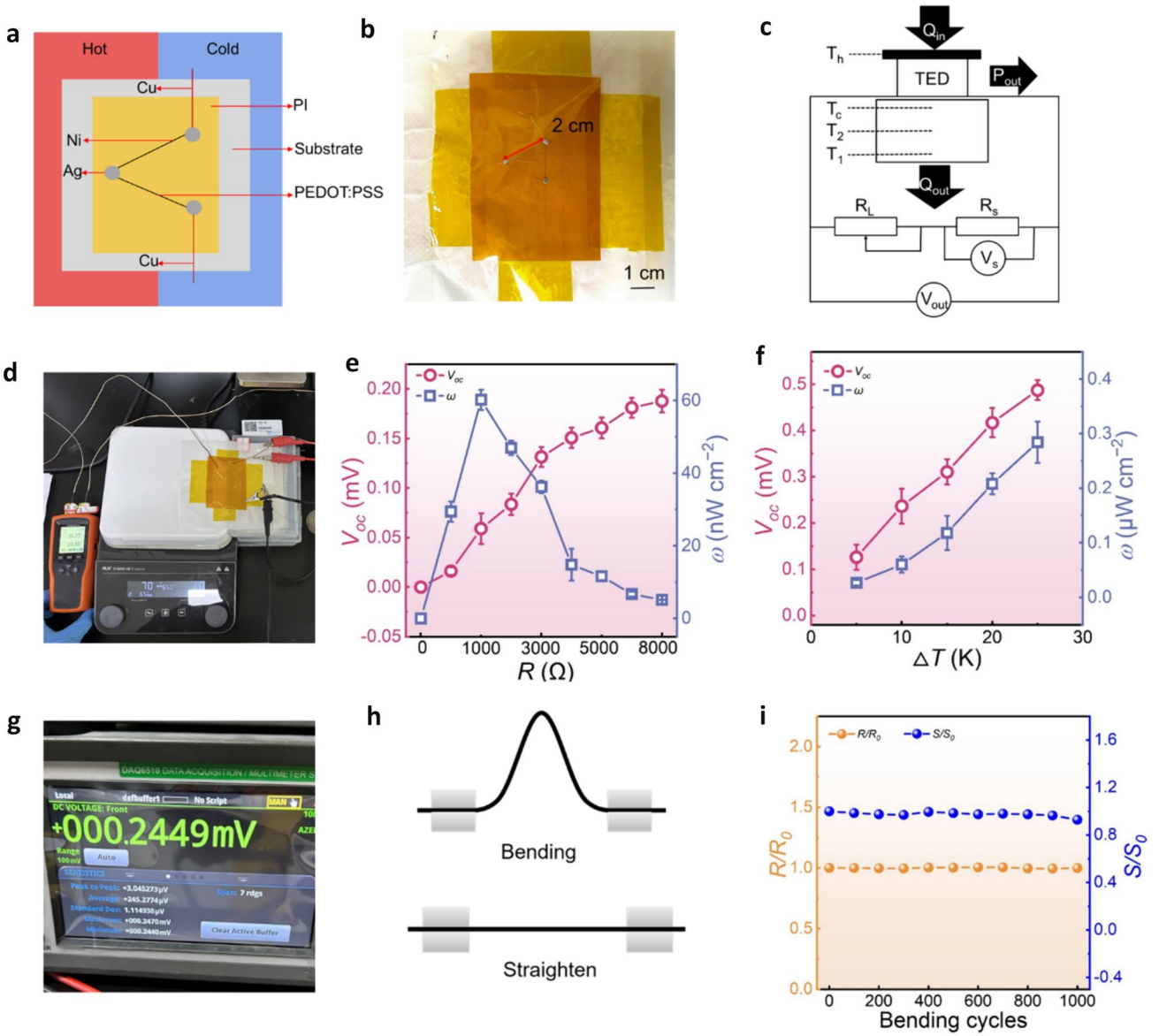

Fig. 6 Deviceization of the fibers. **a** Schematic diagram and **b** photograph of a TED consisting of one couple of thermoelectric legs reasonably post-treated PEDOT:PSS fibers and output performance test. One couple of legs is connected by silver paste. **c** Schematic diagram of the circuit of a TED for output performance test. **d** Photograph to demonstrate the open-circuit voltage (V_{OC}) measurement with the as-designed device placed on the heating table. **e** V_{OC} and output power density versus external resistance at 10 K. **f** V_{OC} and maximum power density of one couple of legs at various ΔTs. **g** Photograph of the V_{OC} test at 10 K. **h** Schematic diagram of bending stability test process. **i** Relative S and resistance R change (described as S/S_0 and R/R_0) of H_2SO_4-$NaBH_4$-EMIM:DCA/CH_3OH-treated PEDOT:PSS fibers after repeated bending

to (1395.5 ± 31.5) S cm^{-1} through H_2SO_4 treatment and EMIM:DCA treatment. $NaBH_4$ treatment at the optimized processing time raised the S from (14.1 ± 0.4) to (20.8 ± 0.8) μV K^{-1}. Benefiting from the contributions of H_2SO_4, $NaBH_4$, and EMIM:DCA/CH_3OH, a power factor of (55.4 ± 1.8) μW m^{-1} K^{-2} was optimized. Both H_2SO_4 and EMIM:DCA/CH_3OH treatments aided in the targeted elimination of excess PSS, serving as the internal insulating domains. Simultaneously, these treatments induced conformational changes in PEDOT chains from benzoyl to quinone characteristics through the oxidative dehydrogenation reaction. At the microstructure level, acid and ionic liquid treatment resulted in highly ordered layer-stacking structures, ensuring high charge carrier mobility, thus yielding an ultra-high σ. $NaBH_4$ treatment, as the second process, optimized thermoelectric performance by adjusting the oxidation level. Additionally, p-n fiber-based TED is assembled for a quantitative evaluation of thermal

collection efficiency. At a ΔT of 25 K, the device demonstrated a satisfactory output voltage of (0.49 ± 0.02) mV, particularly noteworthy for its high power density of up to (0.28 ± 0.04) μW cm^{-2}, owing to the relatively small effective device area. This work offers inspiration for the development of high-performance PEDOT:PSS fiber-based wearable thermoelectric energy harvesting systems.

Supplementary Information The online version contains supplementary material available at https://doi.org/10.1007/s42765-024-00441-5.

Acknowledgements Yu-Yu Deng and Xiao-Lei Shi contributed equally to this work. This work was financially supported by the National Natural Science Foundation of China (No. 52272040), the State Key Laboratory of Materials-Oriented Chemical Engineering Program (SKL-MCE-23A04), the Priority Academic Program Development of Jiangsu Higher Education Institutions (PAPD), and the Jiangsu Specially-Appointed Professor Program. ZGC thanks the financial support from the Australian Research Council, HBIS-UQ Innovation Centre for Sustainable Steel project, and QUT Capacity Building Professor Program. The authors would like to thank the Institute of Coal Chemistry for the test of mechanical properties. This work was enabled by the use of the Central Analytical Research Facility hosted by the Institute for Future Environments at QUT.

Funding Open Access funding enabled and organized by CAUL and its Member Institutions.

Data availability Data will be provided if required in the future.

Declarations

Conflicts of Interest The authors declare that they have no known competing financial interests or personal relationships that could have appeared to influence the work reported in this paper.

References

1. Shi XL, Cao T, Chen W, Hu B, Sun S, Liu WD, Li M, Lyu W, Hong M, Chen ZG. Advances in flexible inorganic thermoelectrics. *EcoEnergy*. **2023**;*1*:296–343.
2. Yang Q, Yang S, Qiu P, Peng L, Wei T-R, Zhang Z, Shi X, Chen L. Flexible thermoelectrics based on ductile semiconductors. *Science*. **2022**;*377*:854–8.
3. Jiang B, Yu Y, Cui J, Liu X, Xie L, Liao J, Zhang Q, Huang Y, Ning S, Jia B, Zhu B, Bai S, Chen L, Pennycook Stephen J, He J. High-entropy-stabilized chalcogenides with high thermoelectric performance. *Science*. **2021**;*371*:830–4.
4. Liu D, Wang D, Hong T, Wang Z, Wang Y, Qin Y, Su L, Yang T, Gao X, Ge Z, Qin B, Zhao L-D. Lattice plainification advances highly effective SnSe crystalline thermoelectrics. *Science*. **2023**;*380*:841–6.
5. Roychowdhury S, Ghosh T, Arora R, Samanta M, Xie L, Singh Niraj K, Soni A, He J, Waghmare Umesh V, Biswas K. Enhanced atomic ordering leads to high thermoelectric performance in $AgSbTe_2$. *Science*. **2021**;*371*:722–7.
6. Shi X-L, Sun S, Wu T, Tu J, Zhou Z, Liu Q, Chen Z-G. Weavable thermoelectrics: advances, controversies, and future developments. *Mater Futures*. **2024**;*3*:012103.
7. Massonnet N, Carella A, Jaudouin O, Rannou P, Laval G, Celle C, Simonato JP. Improvement of the Seebeck coefficient of PEDOT:PSS by chemical reduction combined with a novel method for its transfer using free-standing thin films. *J Mater Chem C*. **2014**;*2*:1278–83.
8. Xu S, Shi XL, Dargusch M, Di C, Zou J, Chen ZG. Conducting polymer-based flexible thermoelectric materials and devices: from mechanisms to applications. *Prog Mater Sci*. **2021**;*121*:100840.
9. Gueye MN, Carella A, Faure-Vincent J, Demadrille R, Simonato J-P. Progress in understanding structure and transport properties of PEDOT-based materials: a critical review. *Prog Mater Sci*. **2020**;*108*:100616.
10. Okuzaki H, Harashina Y, Yan H. Highly conductive PEDOT/PSS microfibers fabricated by wet-spinning and dip-treatment in ethylene glycol. *Eur Polym J*. **2009**;*45*:256–61.
11. Kim J, Jang JG, Hong JI, Kim SH, Kwak J. Sulfuric acid vapor treatment for enhancing the thermoelectric properties of PEDOT:PSS thin-films. *J Mater Sci-Mater El*. **2016**;*27*:6122–7.
12. Liu X, Shi XL, Zhang L, Liu WD, Yang Y, Chen ZG. One-step post-treatment boosts thermoelectric properties of PEDOT:PSS flexible thin films. *J Mater Sci Technol*. **2023**;*132*:81–9.
13. Tu S, Tian T, Lena Oechsle A, Yin S, Jiang X, Cao W, Li N, Scheel MA, Reb LK, Hou S, Bandarenka AS, Schwartzkopf M, Roth SV, Müller-Buschbaum P. Improvement of the thermoelectric properties of PEDOT:PSS films *via* DMSO addition and DMSO/salt post-treatment resolved from a fundamental view. *Chem Eng J*. **2022**;*429*:132295.
14. Zhang M, Cao X, Wen M, Chen C, Wen Q, Fu Q, Deng H. Highly electrical conductive PEDOT:PSS/SWCNT flexible thermoelectric films fabricated by a high-velocity non-solvent turbulent secondary doping approach. *ACS Appl Mater Interfaces*. **2023**;*15*:10947–57.
15. Li B, Yue S, Cheng H, Wu C, Ouyang J. Visible light-induced enhancement in the Seebeck coefficient of PEDOT:PSS composites with two-dimensional potassium poly-(heptazine imide). *J Mater Chem A*. **2022**;*10*:862–71.
16. Kim JY, Lee W, Kang YH, Cho SY, Jang KS. Wet-spinning and post-treatment of CNT/PEDOT:PSS composites for use in organic fiber-based thermoelectric generators. *Carbon*. **2018**;*133*:293–9.
17. Xu H, Guo Y, Wu B, Hou C, Zhang Q, Li Y, Wang H. Highly integrable thermoelectric fiber. *ACS Appl Mater Interfaces*. **2020**;*12*:33297–304.
18. Wen N, Fan Z, Yang S, Zhao Y, Cong T, Xu S, Zhang H, Wang J, Huang H, Li C, Pan L. Highly conductive, ultra-flexible, and continuously processable PEDOT:PSS fibers with high thermoelectric properties for wearable energy harvesting. *Nano Energy*. **2020**;*78*:105361.
19. Lv D, Zheng S, Cao C, Li K, Ai L, Li X, Yang Z, Xu Z, Yao X. Defect-enhanced selective ion transport in an ionic nanocomposite for efficient energy harvesting from moisture. *Energy Environ Sci*. **2022**;*15*:2601–9.
20. Rong L, Xie X, Yuan W, Fu Y. Superior, environmentally tolerant, flexible, and adhesive poly(ionic liquid) gel as a

multifaceted underwater sensor. *ACS Appl Mater Interfaces*. **2022**;*14*:29273–83.
21. Xiang S, He X, Zheng F, Lu Q. Multifunctional flexible sensors based on ionogel composed entirely of ionic liquid with long alkyl chains for enhancing mechanical properties. *Chem Eng J*. **2022**;*439*:135644.
22. Zhu H, Li L, Shi M, Xiao P, Liu Y, Yan X. Coupling of graphene quantum dots with MnO_2 nanosheets for boosting capacitive storage in ionic liquid electrolyte. *Chem Eng J*. **2022**;*437*:135301.
23. Zhao C, Zhang C, Wang P, Chen Z, Wang Y, Zhu J, Gao C, Gao Q. Wet-spun PEDOT:PSS/ionic liquid composite fibers for wearable e-textiles. *Eur Polym J*. **2023**;*190*:112025.
24. Chen H, Xu H, Luo M, Wang W, Qing X, Lu Y, Liu Q, Yang L, Zhong W, Li M, Wang D. Highly conductive, ultrastrong, and flexible wet-spun PEDOT:PSS/ionic liquid fibers for wearable electronics. *ACS Appl Mater Interfaces*. **2023**;*15*:20346–57.
25. Sarabia-Riquelme R, Shahi M, Brill JW, Weisenberger MC. Effect of drawing on the electrical, thermoelectrical, and mechanical properties of wet-spun PEDOT:PSS fibers. *ACS Appl Polym Mater*. **2019**;*1*:2157–67.
26. Zhang J, Seyedin S, Qin S, Lynch PA, Wang Z, Yang W, Wang X, Razal JM. Fast and scalable wet-spinning of highly conductive PEDOT:PSS fibers enables versatile applications. *J Mater Chem A*. **2019**;*7*:6401–10.
27. Liu J, Jia Y, Jiang Q, Jiang F, Li C, Wang X, Liu P, Liu P, Hu F, Du Y, Xu J. Highly conductive hydrogel polymer fibers toward promising wearable thermoelectric energy harvesting. *ACS Appl Mater Interfaces*. **2018**;*10*:44033–40.
28. Ge R, Dong X, Sun L, Hu L, Liu T, Zeng W, Luo B, Jiang X, Jiang Y, Zhou Y. Meters-long, sewable, wearable conductive polymer wires for thermoelectric applications. *J Mater Chem C*. **2020**;*8*:1571–6.
29. Kim Y, Lund A, Noh H, Hofmann AI, Craighero M, Darabi S, Zokaei S, Park JI, Yoon M-H, Müller C. Robust PEDOT:PSS wet-spun fibers for thermoelectric textiles. *Macromol Mater Eng*. **2020**;*305*:1900749.
30. Pan Y, Song Y, Jiang Q, Jia Y, Liu P, Song H, Liu G. Solvent treatment of wet-spinning PEDOT:PSS fiber towards wearable thermoelectric energy harvesting. *Synth Met*. **2022**;*283*:116969.
31. Liu L, Chen J, Liang L, Deng L, Chen G. A PEDOT:PSS thermoelectric fiber generator. *Nano Energy*. **2022**;*102*:107678.
32. Kim N, Kee S, Lee SH, Lee BH, Kahng YH, Jo YR, Kim BJ, Lee K. Highly conductive PEDOT:PSS nanofibrils induced by solution-processed crystallization. *Adv Mater*. **2014**;*26*:2268–72.
33. Aasmundtveit KE, Samuelsen EJ, Pettersson LAA, Inganäs O, Johansson T, Feidenhans'l R. Structure of thin films of poly(3,4-ethylenedioxythiophene). *Synthetic Met*. **1999**;*101*:561–4.
34. Kim N, Lee BH, Choi D, Kim G, Kim H, Kim JR, Lee J, Kahng YH, Lee K. Role of interchain coupling in the metallic state of conducting polymers. *Phys Rev Lett*. **2012**;*109*:106405.
35. Sarabia-Riquelme R, Andrews R, Anthony JE, Weisenberger MC. Highly conductive wet-spun PEDOT:PSS fibers for applications in electronic textiles. *J Mater Chem C*. **2020**;*8*:11618–30.
36. Wang X, Kyaw AKK, Yin C, Wang F, Zhu Q, Tang T, Yee PI, Xu J. Enhancement of thermoelectric performance of PEDOT:PSS films by post-treatment with a superacid. *RSC Adv*. **2018**;*8*:18334–40.
37. Wu T, Shi XL, Liu WD, Sun S, Liu Q, Chen ZG. Dual post-treatments boost thermoelectric performance of PEDOT:PSS films and their devices. *Macromol Mater Eng*. **2022**;*307*:2200411.
38. Garreau S, Louarn G, Buisson JP, Froyer G, Lefrant S. *In situ* spectroelectrochemical Raman studies of poly(3,4-ethylenedioxythiophene) (PEDT). *Macromolecules*. **1999**;*32*:6807–12.
39. Łapkowski M, Proń A. Electrochemical oxidation of poly(3,4-ethylenedioxythiophene)—"*in situ*" conductivity and spectroscopic investigations. *Synthetic Met*. **2000**;*110*:79–83.
40. Wang X, Ge MQ, Feng GY. The effects of DMSO on structure and properties of PVA/PEDOT:PSS blended fiber. *Fiber Polym*. **2015**;*16*:2578–85.
41. Luo J, Billep D, Blaudeck T, Sheremet E, Rodriguez RD, Zahn DRT, Toader M, Hietschold M, Otto T, Gessner T. Chemical post-treatment and thermoelectric properties of poly(3,4-ethylenedioxylthiophene):poly(styrenesulfonate) thin films. *J Appl Phys*. **2014**;*115*:054908.
42. Ouyang J, Chu CW, Chen FC, Xu Q, Yang Y. High-cnductivity poly(3,4-ethylenedioxythiophene):poly(styrene sulfonate) film and its application in polymer optoelectronic devices. *Adv Funct Mater*. **2005**;*15*:203–8.
43. Wang Y, Yang L, Shi X, Shi X, Chen L, Dargusch M, Zou J, Chen Z-G. Flexible thermoelectric materials and generators: Challenges and innovations. *Adv Mater*. **2019**;*31*:1807916.
44. Crispin X, Jakobsson FLE, Crispin A, Grim PCM, Andersson P, Volodin A, van Haesendonck C, Van der Auweraer M, Salaneck WR, Berggren M. The origin of the high conductivity of poly(3,4-ethylenedioxythiophene)-poly(styrenesulfonate) (PEDOT-PSS) plastic electrodes. *Chem Mater*. **2006**;*18*:4354–60.
45. Kim GH, Shao L, Zhang K, Pipe KP. Engineered doping of organic semiconductors for enhanced thermoelectric efficiency. *Nat Mater*. **2013**;*12*:719–23.
46. Massonnet N, Carella A, de Geyer A, Faure-Vincent J, Simonato J-P. Metallic behaviour of acid doped highly conductive polymers. *Chem Sci*. **2015**;*6*:412–7.
47. van Reenen S, Scheepers M, van de Ruit K, Bollen D, Kemerink M. Explaining the effects of processing on the electrical properties of PEDOT:PSS. *Org Electron*. **2014**;*15*:3710–4.
48. Fan Z, Li P, Du D, Ouyang J. Significantly enhanced thermoelectric properties of PEDOT:PSS films through sequential post-treatments with common acids and bases. *Adv Energy Mater*. **2017**;*7*:1602116.
49. Bubnova O, Berggren M, Crispin X. Tuning the thermoelectric properties of conducting polymers in an electrochemical transistor. *J Am Chem Soc*. **2012**;*134*:16456–9.
50. Zozoulenko I, Singh A, Singh SK, Gueskine V, Crispin X, Berggren M. Polarons, bipolarons, and absorption spectroscopy of PEDOT. *ACS Appl Polym Mater*. **2019**;*1*:83–94.
51. Lee I, Kim GW, Yang M, Kim TS. Simultaneously enhancing the cohesion and electrical conductivity of PEDOT:PSS conductive polymer films using DMSO additives. *ACS Appl Mater Interfaces*. **2016**;*8*:302–10.
52. Fan X, Nie W, Tsai H, Wang N, Huang H, Cheng Y, Wen R, Ma L, Yan F, Xia Y. PEDOT:PSS for flexible and stretchable electronics: modifications, strategies, and applications. *Adv Sci*. **2019**;*6*:1900813.
53. Jalili R, Razal JM, Innis PC, Wallace GG. One-step wet-spinning process of poly(3,4-ethylenedioxythiophene):poly(styrene sulfonate) fibers and the origin of higher electrical conductivity. *Adv Funct Mater*. **2011**;*21*:3363–70.
54. Park H, Lee SH, Kim FS, Choi HH, Cheong IW, Kim JH. Enhanced thermoelectric properties of PEDOT:PSS nanofilms by a chemical dedoping process. *J Mater Chem A*. **2014**;*2*:6532–9.
55. Döbbelin M, Marcilla R, Salsamendi M, Pozo-Gonzalo C, Carrasco PM, Pomposo JA, Mecerreyes D. Influence of ionic liquids on the electrical conductivity and morphology of PEDOT:PSS films. *Chem Mater*. **2007**;*19*:2147–9.
56. Badre C, Marquant L, Alsayed AM, Hough LA. Highly conductive poly(3,4-ethylenedioxythiophene):poly (styrenesulfonate)

films using 1-ethyl-3-methylimidazolium tetracyanoborate ionic liquid. *Adv Funct Mater*. **2012**;*22*:2723–7.
57. Teo MY, Kim N, Kee S, Kim BS, Kim G, Hong S, Jung S, Lee K. Highly stretchable and highly conductive PEDOT:PSS/ionic liquid composite transparent electrodes for solution-processed stretchable electronics. *ACS Appl Mater Interfaces*. **2017**;*9*:819–26.
58. Atoyo J, Burton MR, McGettrick J, Carnie MJ. Enhanced electrical conductivity and Seebeck coefficient in PEDOT:PSS *via* a two-step ionic liquid and $NaBH_4$ treatment for organic thermoelectrics. *Polymers*. **2020**;*12*:559.
59. Al-Nimr MDA, Tashtoush BM, Jaradat AA. Modeling and simulation of thermoelectric device working as a heat pump and an electric generator under Mediterranean climate. *Energy*. **2015**;*90*:1239–50.
60. Fang H, Popere BC, Thomas EM, Mai CK, Chang WB, Bazan GC, Chabinyc ML, Segalman RA. Large-scale integration of flexible materials into rolled and corrugated thermoelectric modules. *J Appl Polym Sci*. **2017**;*134*:44208.
61. Beretta D, Massetti M, Lanzani G, Caironi M. Thermoelectric characterization of flexible micro-thermoelectric generators. *Rev Sci Instrum*. **2017**;*88*:015103.
62. Li C, Sun P, Liu C, Xu J, Wang T, Wang W, Hou J, Jiang F. Fabrication of flexible SWCNTs-Te composite films for improving thermoelectric properties. *J Alloys Compd*. **2017**;*723*:642–8.
63. Wang X, Meng F, Wang T, Li C, Tang H, Gao Z, Li S, Jiang F, Xu J. High performance of PEDOT:PSS/SiC-NWs hybrid thermoelectric thin film for energy harvesting. *J Alloys Compd*. **2018**;*734*:121–9.